Bisindolylmaleimides as Red Electroluminescence Materials

Ching-Wen Chiu, Tahsin J. Chow,* Chang-Hao Chuen, Hsiu-Mei Lin, and Yu-Tai Tao

Institute of Chemistry, Academia Sinica, Taipei, Taiwan, 115

Received May 12, 2003. Revised Manuscript Received September 9, 2003

Derivatives of bisindolylmaleimide were found to form amorphous solid films which exhibit red luminescence, and can be fabricated into light-emitting diodes. The property of forming glasses can be ascribed to the nonplanar geometry of these molecules. Single-crystal X-ray diffraction analyses revealed the presence of pseudo *E* and *Z* conformational isomers which are responsible for the phenomena of polymorphism detected by differential scanning calorimetry. All compounds exhibit distinct glass transition temperatures, and several show dual melting temperatures. Two kinds of devices were fabricated in which a layer of pure dye was sandwiched between opposite charge transporting layers. The emission spectra of devices utilizing tris(8-hydoxyquinolinato)aluminum (Alq) contained a green component from Alq. Pure red emissions can be achieved by replacing Alq with 2,2′,2″-(1,3,5-benzenetriyl)-tris(1-phenyl-1H-benzimidazole) (TPBI). Typical devices can be turned on at about 3 V with maximal intensity of ∼2000 cd/m^2.

Introduction

Designing organic materials for the fabrication of light-emitting diodes (LED) has been an area of intensive research interest.[1,2] The fabrication of multilayer structures and the usage of dopants have been quite successful for producing LED devices of high quantum efficiency and color tunability.[3−5] For full color display, chromaticity control over the whole visible range is required. Materials exhibiting intense green and blue colors are abundant, but red luminescence materials are scarce.[6−8] Organic red dyes are usually polar molecules which tend to crystallize in the solid state, therefore they self-quench their luminescence. Most of these dyes exhibit broad, orange-red emission with low photochemical stability.[3,9] Although sharp red emission may be achieved by using rare-earth complexes, those devices yielded poor quantum efficiency.[6,10] The most successful red-emitting devices so far are fabricated by doping red dyes in inert host matrixes.[11] Nondopant type red-emitting materials are rare, and were reported only recently.[7,8]

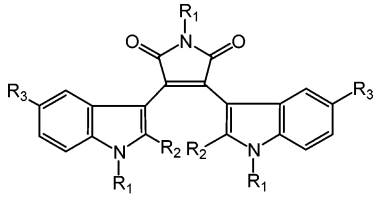

1) $R_1 = R_2 = CH_3$; $R_3 = H$
2) $R_1 = R_2 = CH_3$; $R_3 = OCH_3$
3) $R_1 = CH_3$; $R_2 = Ph$; $R_3 = H$
4) $R_1 = CH_2CH_3$; $R_2 = CH_3$; $R_3 = H$

Bisindolylmaleimides **1**−**4** are derivatives of Arcyriarubins A (all R's = H) which belongs to a family of pigments produced by the slime molds (*Myxomycetes*).[12] This class of compounds has also been used widely as photochromic materials because of their reversible 6π-cyclization reactions.[13] In our continuous search of

* To whom correspondence should be addressed. Fax: (886)-2-27884179. E-mail: tjchow@chem.sinica.edu.tw.

(1) (a) Miyata, S., Nalwa, H. S., Eds. *Organic Electroluminescent Materials and Devices*; Gordon and Breach: Amsterdam, The Netherlands, 1997. (b) *Acc. Chem. Res.* **1999**, *32*, 191 (Special issue on Molecular Materials in Electronics and Optoelectronic Devices). (c) Ishii, H.; Sugiyama, K.; Ito, E.; Seki, K. *Adv. Mater.* **1999**, *11*, 605.

(2) Tang, C. W.; VanSlyke, S. A. *Appl. Phys. Lett.* **1987**, *51*, 913.

(3) Tang, C. W.; Van Slyke, S. A.; Chen, C. H. *J. Appl. Phys.* **1989**, *65*, 3610.

(4) (a) Adachi, C.; Tokito, S.; Tsutsui, T.; Saito, S. *Jpn. J. Appl. Phys. Part 2* **1988**, *27*, 269. (b) Hosokawa, C.; Higashi, H.; Nakamura, H.; Kusumoto, T. *Appl. Phys. Lett.* **1995**, *67*, 3853. (c) Gao, Z. Q.; Lee, C. S.; Bello, I.; Lee, S. T.; Chen, R. M.; Lu, T. Y.; Shi, J.; Tang, C. W. *Appl. Phys. Lett.* **1999**, *74*, 865.

(5) Chow, T. J.; Lin, R.; Ko, C.-W.; Tao, Y.-T. *J. Mater. Chem.* **2002**, *12*, 42.

(6) (a) Okada, K.; Wang, Y.−F.; Chen, T.-M.; Kitamura, M.; Nakaya, T.; Inoue, H. *J. Mater. Chem.* **1999**, *9*, 3023. (b) Kido, J.; Endo, J. *Chem. Lett.* **1997**, 633. (c) Picciolo, L. C.; Murata, H.; Kafafi, Z. H. *Appl. Phys. Lett.* **2001**, *78*, 2378.

(7) Wu, W.-C.; Yeh, H.-C.; Chan, L.-H.; Chen, C.-T. *Adv. Mater.* **2002**, *14*, 1072.

(8) Thomas, K. R. J.; Lin, J. T.; Tao, Y. T.; Chuen, C.-H. *Adv. Mater.* **2002**, *14*, 822.

(9) (a) Bulovic, V.; Shoustikov, A.; Baldo, M. A.; Bose, E.; Kozlov, V. G.; Thompson, M. E.; Forrest, S. R. *Chem. Phys. Lett.* **1998**, *287*, 455. (b) Tao, X. T.; Miyata, S.; Sasabe, H.; Zhang, G. J.; Wada, T.; Jiang, M. H. *Appl. Phys. Lett.* **2001**, *78*, 279.

(10) (a) Kido, J.; Hayase, H.; Hongawa, K.; Nagai, K.; Okuyama, K. *Appl. Phys. Lett.* **1994**, *85*, 2124. (b) Adachi, C.; Baldo, M. A.; Forrest, S. R. *J. Appl. Phys.* **2000**, *87*, 8049.

(11) (a) Xie, Z. Y.; Hung, L. S.; Lee, S. T. *Appl. Phys. Lett.* **2001**, *79*, 1048. (b) Liu, H.; Gao, W.; Yang, K.; Chen, B.; Liu, S.; Bai, Y. *Chem. Phys. Lett.* **2002**, *352*, 353. (c) Shoustikov, A.; You, Y.; Burrows, P. E.; Thompson, M. E.; Forrest, S. R. *Synth. Met.* **1997**, *91*, 217. (d) Hamada, Y.; Kanno, H.; Tsujoika, T.; Takahashi, H.; Usuki, T. *Appl. Phys. Lett.* **1999**, *75*, 1682.

(12) Steglich, W.; Steffan, B.; Kopanski, L.; Eckhardt, G. *Angew. Chem.* **1980**, *92*, 463; *Angew. Chem., Int. Ed. Engl.* **1980**, *19*, 459.

10.1021/cm0303890 CCC: $25.00
Published on Web 10/18/2003

applicable organic LED materials,[5] we found that these compounds yielded bright red luminescence both in solutions and in the solid state. The conjugated chromophore in these compounds cannot keep a planar geometry because ofsteric hindrance of the two vicinal indole groups. The nonplanar conformation is likely to induce an easy formation of amorphous glass in solid film, especially when bulky substituents appeared at C(2′) and C(2″) positions. The steric effect is analyzed by changing substituents, whereas the crystal structures of **1** and **4** were examined by X-ray diffraction analyses.

All four dyes (**1**−**4**) exhibit electroluminescence (EL) while fabricated into LED devices. Two kinds of devices were examined in this study: ITO/NPB/dye/Alq/Mg:Ag (type A) and ITO/NPB/dye/TPBI/Mg:Ag (type B), where ITO denotes indium−tin oxide, NPB = 4,4′-bis[*N*-(1-naphthyl)*N*-phenylamino]biphenyl, Alq = tris(8-hydoxyquinolinato)aluminum), and TPBI = 2,2′,2″-(1,3,5-benzenetriyl)tris(1-phenyl-1H-benzimidazole.

Experimental Section

General. Absorption spectra were taken on a Hewlett-Packard 8453 spectrophotometer, and emission spectra were obtained on a Hitachi F-4500 fluorescence spectrophotometer. ^{1}H and ^{13}C NMR spectra were recorded on a VXM-300/50 superconducting FT NMR spectrometer. Mass spectra were taken on a Joel JMS SX/SX 102A spectrometer. Microanalyses were completed on a Heraeus CHNOS Rapid F002 elemental analyzer. X-ray diffraction analyses were done on a Brucker AXS SMART-1000 spectrometer. Cyclic voltammetry measurements were carried out on a BAS 100B electrochemical analyzer equipped with a conventional three-electrodes system (i.e., glassy carbon, platinum wire, and Ag/AgCl as working, counter, and reference electrodes, respectively). Degassed dichloromethane solution with 0.1 M tetra-*n*-butylammonium hexafluorophosphate was used as electrolyte.

Device Fabrication. ITO-coated glass with sheet resistance of <50 Ω/□ was used as substrate. The substrate was pre-patterned by photolithography to give an effective device size of 3.14 mm^2. Pretreatment of ITO included a routine chemical cleaning using detergent and alcohol in sequence, followed by oxygen plasma cleaning. Thermal evaporation of organic materials was carried out using ULVAC Cryogenics at a chamber pressure of 10^{-6} Torr. Two types of devices were configured as ITO/NPB (40 nm)/dye (10 nm)/Alq (40 nm)/Mg:Ag and ITO/NPB (40 nm)/dye (10 nm)/TPBI (40 nm)/Mg:Ag. Coevaporation of Mg and Ag into an alloy $Mg_{0.9}Ag_{0.1}$ (50 nm) was used as the cathode, which was capped by a thick layer of silver. Current voltage and light intensity measurements were done on a Keithley 2400 Source meter and a Newport 1835C Optical meter equipped with a Newport 818-ST silicon photodiode, respectively. All measurements were completed under ambient conditions.

General Procedure for Syntheses. All compounds were prepared according to known procedures.[14] To a toluene (150 mL) solution of 2-substituted indole (40 mmol) was added MeMgCl (3 M in THF, 48 mmol) at room temperature under a nitrogen atmosphere, and the solution was heated 60 °C for 1 h. To it a solution of dibromomaleimide (8 mmol) in toluene (20 mL) was then added, and the mixture was heated to reflux for 24−72 h. The reaction was monitored by thin layer chromatograph till completion. The mixture was cooled to room temperature, and was diluted with ethyl acetate (250 mL). The combined organic part was washed with HCl (1.0 N, 100 mL), water (100 mL), and brine (100 mL) in succession, and was dehydrated over anhydrous $MgSO_4$. It was dried in vacuo to form a dark red residue. The crude product was purified through silica gel column chromatograph eluted with ethyl acetate/hexane (1:1), and was subjected to the next step.

N-Alkylation was done by first deprotonation of bis-indolylmaleimide (3 mmol) in DMF (15 mL) with NaH (9 mmol). To the mixture was added iodo-methane or iodo-ethane (11 mmol) dropwise, then it was stirred with a magnetic bar at room temperature for 1 h. The reaction was quenched by the addition of water (1.0 L), and was filtered. The filtrate was recrystallized from CH_2Cl_2 and hexane to yield bright red crystalline solids.

2,3-Bis(2′,*N*-dimethyl-3′-indolyl)-*N*-methylmaleimide (1). Physical data of **1** (yield 85%). Anal. Calcd for $C_{25}H_{23}N_3O_2$: C, 75.54; H, 5.83; N, 10.57. Found: C, 75.95; H, 5.90; N, 10.45. ^{1}H NMR (CD_2Cl_2, 400 MHz) δ 2.07 (s, 6H), 3.17 (s, 3H), 3.60 (s, 6H), 6.90 (t, 7 Hz, 2H), 7.10 (m & t, 7.5 Hz, 2H), 7.25 (d, 7.5 Hz, 2H). ^{13}C NMR (CD_2Cl_2, 100 MHz, H-decoupled) δ 12.50, 24.53, 30.31, 104.33, 109.47, 120.40, 126.74, 122.21, 126.74, 132.60, 137.74, 138.98, 172.41. IR (KBr, cm^{-1}): 3048 (w), 2940 (w), 2901 (w), 1754 (m), 1705 (s), 1612 (m), 1538 (m), 1435 (s), 1381 (s), 739(s). MS (FAB) *m/e* 397 (M$^+$, 100%), 297 (47).

2,3-Bis(2′,*N*-dimethyl-5′-methoxy-3′-indolyl)-*N*-methylmaleimide (2). Physical data of **2** (yield 72%). Anal. Calcd for $C_{27}H_{27}N_3O_4$: C, 70.88; H, 5.95; N, 9.18. Found: C, 70.84; H, 5.96; N, 8.85. ^{1}H NMR ($CDCl_3$, 400 MHz) δ 2.08 (br, 6H), 3.20 (s, 3H), 3.34 (br, 6H), 3.51 (s, 6H), 6.50 (s, 2H), 6.69 (m, 2H), 7.02 (d, 8.5 Hz, 2H). ^{13}C NMR ($CDCl_3$, 100 MHz, H-decoupled) δ 12.50, 24.42, 30.05, 55.32, 101.85, 104.12, 109.69, 111.96, 126.46, 131.53, 132.42, 138.88, 154.56, 172.17. IR (KBr, cm^{-1}): 2989 (w), 2940 (w), 2828 (w), 1752 (m), 1701 (s), 1617 (m), 1540 (m), 1487 (s), 1436 (s), 1379 (s), 1234 (s), 1155 (s). MS (FAB) *m/e* 457 (M$^+$, 100%), 443 (17).

2,3-Bis(*N*-methyl-2′-phenyl-3′-indolyl)-*N*-methylmaleimide (3). Physical data of **3** (yield 47%). Anal. Calcd for $C_{35}H_{27}N_3O_2$: C, 80.59; H, 5.22; N, 8.06. Found: C, 80.30; H, 5.12; N, 7.95. ^{1}H NMR ($CDCl_3$, 400 MHz) δ 2.98 (br, 3H), 3.44 (br, 6H), 6.60 (br, 4H), 6.76 (br, 2H), 6.94 (br, 2H), 7.05 (br, 2H), 7.19 (br, 8H). ^{13}C NMR ($CDCl_3$, 100 MHz, H-decoupled) δ 24.39, 31.21, 104.77, 109.62, 120.56, 121.12, 122.47, 126.66, 127.92, 127.95, 130.11, 131.94, 132.52, 137.97, 141.75, 171.44. IR (KBr, cm^{-1}): 3046 (w), 2827 (w), 1760 (m), 1697 (s), 1620 (w), 1545 (w), 1468 (s), 1434 (s), 1380 (s), 745 (s). MS (FAB) *m/e* 521 (M$^+$, 27%), 436 (4), 371 (6).

2,3-Bis(*N*-ethyl-2′-methyl-3′-indolyl)-*N*-ethylmaleimide (4). Physical data of **4** (yield 82%). Anal. Calcd for $C_{28}H_{29}N_3O_2$: C, 76.51; H, 6.65; N, 9.56. Found: C, 76.46; H, 6.51; N, 8.40. ^{1}H NMR ($CDCl_3$, 400 MHz) δ 1.17 (t, 8 Hz, 6H), 1.33 (t, 8 Hz, 3H), 1.96 (s, 6H), 3.75 (q, 8 Hz, 3H), 4.02 (q, 8 Hz, 6H), 6.88 (m, 2H), 7.08 (m, 4 H), 7.19 (m, 2H). ^{13}C NMR ($CDCl_3$, 100 MHz, H-decoupled) δ 12.05, 14.37, 14.97, 33.37, 38.10, 104.48, 108.93, 120.23, 120.53, 121.49, 126.36, 131.83, 136.19, 137.45, 171.92. IR (KBr, cm^{-1}): 3043 (w), 2975 (m), 2936 (w), 1753 (m), 1701 (s), 1622 (w), 1536 (s), 1463 (s), 1429 (s), 1399 (s), 1348 (s), 745 (s). MS (FAB) *m/e* 439 (M$^+$, 100%), 425 (5).

Results and Discussion

Physical Properties. Compounds **1**−**4** were prepared by reaction of 3-indolylmagnesium chloride with 2,3-dihalomaleimide. The three NH groups were then alkylated first by deprotonation with sodium hydride, followed by reaction with alkyl iodide. All products were collected as red crystalline solids. In the ^{1}H NMR spectra of **2** and **3** line broadening appeared for the methyl and phenyl signals. The line broadening is ascribed to restricted rotations along C(2)−C(3′) and C(3)−C(3″) bonds (the bond connecting the indole and maleimide moieties as shown in Figure 1). The substituents at C(2′) and C(2″) keep the two indole rings out-

(13) (a) Liang, Y.; Dvornikov, A. S.; Rentzepis, P. M. *J. Mater. Chem.* **2000**, *10*, 2477. (b) Sun, Z,; Hosmane, R. S.; Tadros, M.; Guha, S.; Chen, W.; Chen, J.-M. *J. Heterocyclic Chem.* **1995**, *32*, 1819.

(14) (a) Faul, M. M.; Sullivan, K. A.; Winneroski, L. *Synthesis* **1995**, 1511. (b) Brenner, M.; Rexhausen, H.; Steffan, B.; Steglish, W. *Tetrahedron* **1988**, *44*, 2887.

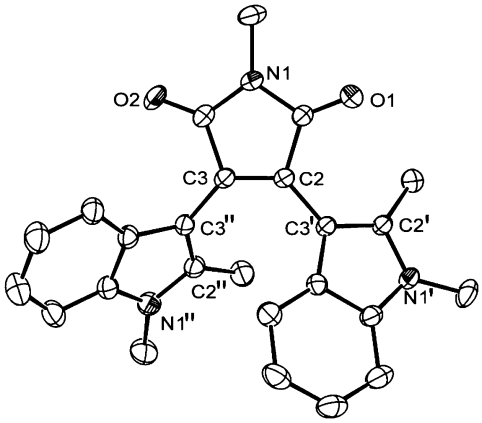

Figure 1. Crystal structure of compound **1** showing the conformation of the indole moieties. Hydrogen atoms are omitted for clarity.

Table 1. Crystal Data and Structure Refinement for Compounds 1 and 4

parameters/compounds	compound **1**	compound **4**
formula	$C_{25}H_{23}N_3O_2$	$C_{28}H_{29}N_3O_2$
formula weight	397.46	439.54
temperature (K)	293(2)	293(2)
wavelength (Å)	0.71073	0.71073
crystal system	triclinic	monoclinic
space group	$P\bar{1}$	$P2_1/n$
cell dimensions (Å)	$a = 8.344(3)$	$a = 11.958(3)$
	$b = 10.043(3)$	$b = 15.402(3)$
	$c = 12.731(4)$	$c = 13.430(3)$
	$\alpha = 82.65(3)°$	$\alpha = 90°$
	$\beta = 88.36(3)°$	$\beta = 92.249(15)°$
	$\gamma = 74.72(2)°$	$\gamma = 90°$
final R indices $[I > 2\sigma(I)]$	$R_1 = 0.0597$	$R_1 = 0.0523$
	$wR_2 = 0.1699$	$wR_2 = 0.1361$
R indices (all data)	$R_1 = 0.1234$	$R_1 = 0.1495$
	$wR_2 = 0.2097$	$wR_2 = 0.1706$

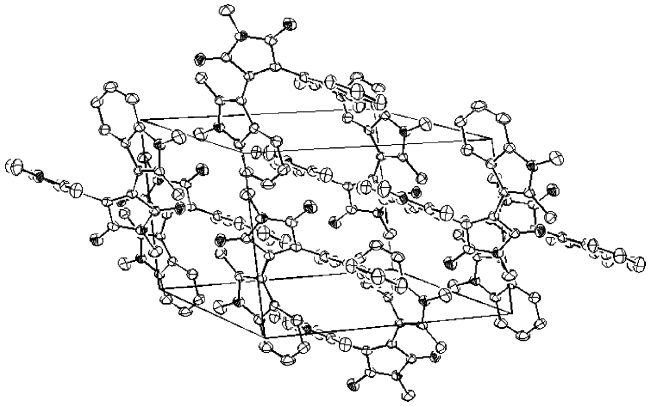

Figure 2. Crystal packing pattern for compound **1** in a unit cell.

of-plane with respect to the π-bond of C(2)═C(3). In the structure of **3**, the phenyl substituents at C(2′) and C(2″)) form two additional out-of-plane twists which make the molecular geometry even more irregular. The line-broadening was less apparent for compounds **1** and **4**, in which the indolyl moieties are less bulky than those of **2** and **3**.

The crystal structures of compounds **1** and **4** were examined by X-ray diffraction analyses. Crystal parameters and refinement data are listed in Table 1. On their crystal drawings (Figures 1 and 3) it is clear that the two indole rings are not coplanar with the ring of

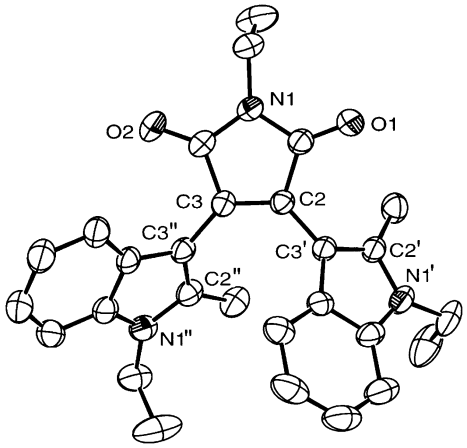

Figure 3. Crystal structure of compound **4** showing the conformation of the indole moieties. Hydrogen atoms are omitted for clarity.

Table 2. Selected Bond Lengths, Angles, and Dihedral Angles around C(2) and C(3) of the Crystal Structures of Compounds 1 and 4

structural parameters[a]	compound **1**	compound **4**
C(2)−C(3)	1.351(4) Å	1.359(3) Å
C(2)−C3′)	1.461(4) Å	1.453(3) Å
C(3)−C(3″)	1.448(4) Å	1.453(3) Å
C(1)−C(2)−C(3′)	121.4(3)°	122.2(2)°
C(3)−C(2)−C(3′)	130.5(3)°	129.8(2)°
C(2)−C(3)−C(3″)	131.4(3)°	131.5(2)°
C(3″)−C(3)−C(4)	121.1(3)°	121.0(2)°
|C(1)−C(2)−C(3′)−C(4′)|	43.2(3)°	46.4(2)°
|C(2)−C(3)−C(3″)−C(4″)|	48.3(3)°	45.6(3)°
|C(3)−C(2)−C(3′)−C(4′)|	36.2(4)°	40.2(4)°
|C(4)−C(3)−C(3″)−C(4″)|	51.6(4)°	46.9(3)°

[a] The numbering of atoms is shown in Figure 1.

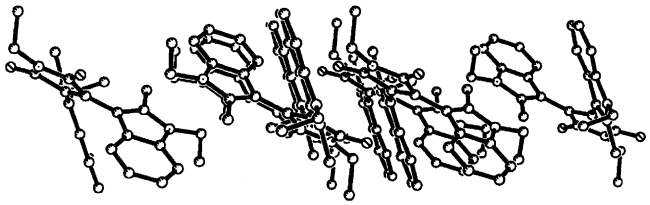

Figure 4. Crystal packing pattern for compound **4** showing relative orientation of the two indole moieties.

maleimide. Rotation across the inner bay region is restricted by steric hindrance between the methyl groups at C(2′) and C(2″). The dihedral angle of C(3)−C(2)−C(3′)−C(4′) of **1** is estimated as 36°, very close to that of C(4″)−C(3′)−C(3)−C(2) (40°) in a symmetrical position (Table 2). However it is noticed that two indole groups are not oriented in the same fashion, i.e., one is aligned in a pseudo-*E* geometry with respect to maleimide while another is in a pseudo-*Z* geometry. The relative orientation of the two indole groups can be more clearly seen in Figures 2 and 4. A conversion from *E* to *Z*, or vice versa, should be responsible for the phenomenon of polymorphism observed on differential scanning calorimetry (DSC).

Certain types of molecular materials may exist in the form of amorphous glass and exhibit polymorphism, i.e., more than one type of crystalline form. The glass is in a thermodynamically nonequilibrium state and may show glass-transition phenomenon which is usually associated with amorphous polymers. Amorphous molecular materials generally possess nonplanar geometry,

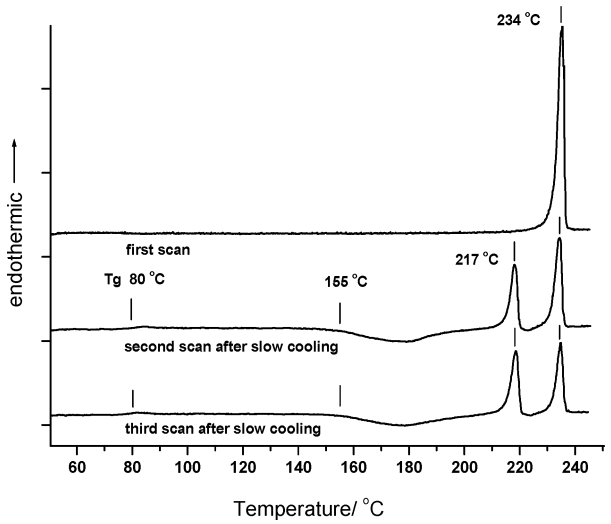

Figure 5. DSC plots of compound **4**. The sample was heated at 20 °C/min during the first scan, then was cooled at the same rate. The process was repeated once again, and the second and third plots exhibited a similar pattern. A glass transition temperature appeared at 80 °C (onset), crystallization at 155 °C (onset), and two melting temperatures with peak maxima at 217 and 234 °C. The behavior is consistent with the formation of molecular amorphous glass, as well as the existence of polymorphism.

Table 3. Temperatures (°C) Measured by DSC at the Onsets of Glass Transition (T_g), Crystallization (T_c), and Melting (T_m)

	T_g	T_c	T_m
1	108	159, 183	301, 332
2	108	190	243
3	122	208	287, 301
4	80	155	210, 226

as that shown on the crystal structure of compounds **1** and **4**. A typical graph of DSC for compound **4** is shown in Figure 5. The compound was heated at a rate of 20 °C/min, while an endothermic peak appeared at 234 °C (onset at 225 °C) which implies the melting of crystals. After a slow cooling process (at 20 °C/min), the same sample was heated again. On the second run a small endothermic hump was detected at 80 °C, which was assigned to a glass transition temperature (T_g). Crystallization happened at 155 °C (T_c) which appeared as a broad exothermic band. It was interesting to observe that two melting peaks appeared at maxima 217 and 234 °C (T_m), respectively. Similar heating behavior was repeated on further scans.

The presence of T_g indicated the existence of amorphous state of this molecular material, thus explaining the unusual high intensity of red luminescence in the solid state. The glass was formed under a slow cooling process, unlike others for which fast cooling (dipping into liquid nitrogen immediately after melting) may be required. The nonplanar geometry and flexible conformation of molecules prevents their efficient crystal packing. The appearance of two crystalline forms can be understood by the existence of pseudo-*E* and pseudo-*Z* conformations as depicted by X-ray diffraction analyses.

Glass-transition phenomena were observed for all compounds **1**−**4**, and T_g values are listed in Table 3. All compounds may form amorphous glasses upon vapor deposition during device fabrications. Compound **3** exhibits the highest T_g (122 °C) among the four, which may be attributed to the bulky phenyl groups at C(2′) and C(2″). Compounds **1**, **3**, and **4** showed dual T_m peaks after the first scan, indicating the formation of two kinds of crystals during solidification. These compounds also showed good thermal stability, as there was no sign of decomposition after heating to 350 °C.

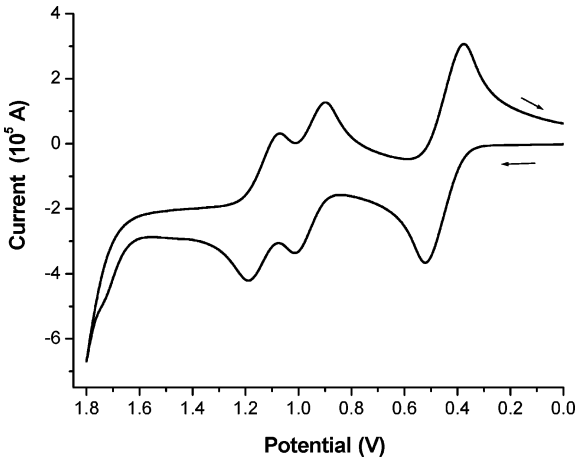

Figure 6. Oxidative CV plot of compound **1**, which exhibited two pairs of reversible waves at 0.96 and 1.13 V. The reversible wave at 0.45 V was ferrocene which was added as an internal standard.

Oxidation potentials of the four compounds were measured by cyclic voltammetry (CV) in methylene chloride using Ag/AgCl as a reference electrode. Each compound of **1**−**4** showed a pair of reversible redox peaks separated by ca. 110 mV (Figure 6). The reversible nature of these peaks indicates the electrochemical stability of these compounds. The half-peak potentials ($E_{1/2} = 1/2(E_{pa} + E_{pc})$) of the first oxidation wave were estimated to be 0.96, 0.96, 0.98, and 0.96 V for **1**−**4**, respectively. The HOMO levels were estimated by a comparison with the ionization potential of ferrocene, which has been determined to be 4.8 eV.[15a,b] The HOMO−LUMO band gap of these compounds in the solid state can be reasonably estimated by the wavelength at which their absorption and emission spectra intersected, i.e., 2.25 eV corresponding to 550 nm.

Absorption and Emission Spectra. The UV spectra of **1**−**4** showed two major absorption bands at λ_{max} 470−475 ($\epsilon = \sim 5 \times 10^3$ in acetonitrile) and 285−290 nm ($\epsilon = \sim 1.0 \times 10^4$), which were assigned to $\pi-\pi^*$ transitions from S_0 to the S_1 and S_2 states, respectively (Figure 7). Irradiating at 475 nm, compounds **1**−**4** exhibit red luminescence at λ_{em} 630−660 nm (Figure 7). Compound **3** shows a slightly greater Stokes shift than the other three, probably due to the more bulky phenyl substituents at C(2′) and C(2″). As the conjugated systems are more twisted out-of-plane, conformational readjustment upon excitation becomes more pronounced. Changing N-substituent from methyl (**1**) to ethyl (**4**) did not result in a significant difference in the spectrum, neither did the presence of an additional

(15) (a) Pommerehne, J.; Vestweber, H.; Guss, W.; Mahrt, R. F.; Bässler, H.; Porsch, M.; Daub, J. *Adv. Mater.* **1995**, *7*, 551. (b) Janietz, S.; Bradley, D. D. C.; Grell, M.; Giebeler, C.; Indasekaran, M.; Woo, E. P. *Appl. Phys. Lett.* **1998**, *73*, 2453. (c) Zhilin, Z.; Xueyin, J.; Shaohong, X. *Thin Solid Films* **2000**, *363*, 61. (d) Gao, Z.; Lee, C. S.; Bello, I.; Lee, S. T.; Chen, R.-M.; Luh, T.-Y.; Shi, J.; Tang, W. *Appl. Phys. Lett.* **1999**, *74*, 865.

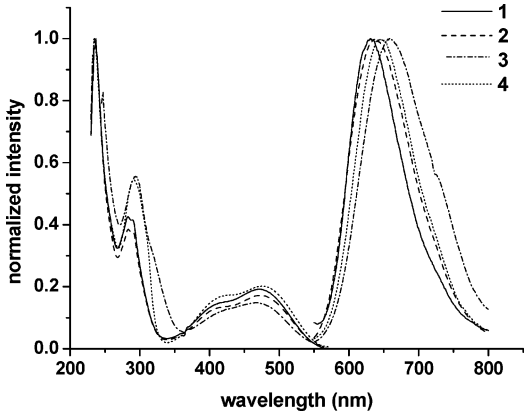

Figure 7. Normalized absorption (left) and emission (right) spectra of **1**−**4**.

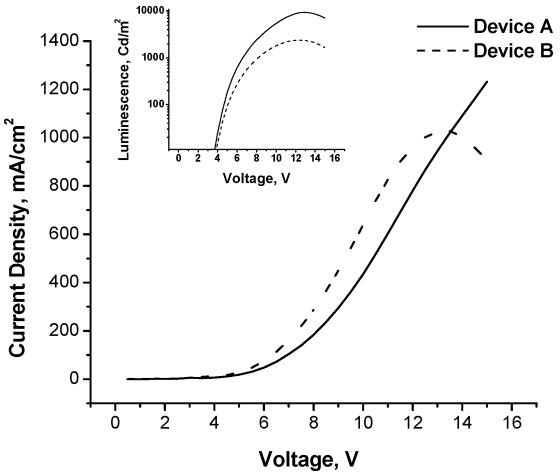

Figure 8. Current (*I*) vs voltage (*V*) plot for the devices of **1** fabricated in both types A and B. The upper inset is a plot of Log(*L*) vs *V*, in which the turn-on voltage (ca. 3.8 V) was clearly indicated.

methoxy group on the indole moieties (at C(5′) and C(5″)) of compound **2**. The property of red-color emission stays intact upon changing substituents, which is an advantage for these materials as it allows us to optimize film morphology during device fabrication by modifying their structures.

Device Fabrication. Two types of devices with configurations of ITO/NPB/dye (**1**−**4**)/Alq/Mg:Ag (device A) and ITO/NPB/dye (**1**−**4**)/TPBI/Mg:Ag (device B) were fabricated for a comparison. A NPB film (40 nm) was vacuum-deposited on ITO glass first, followed by a layer of the dye (**1**−**4**) and another layer of either Alq or TPBI. The devices were completed by coevaporation of a Mg:Ag alloy as cathode, which was capped by a pure Ag layer for electrode contact. The I−V and L−V curves for both devices for compound **1** are shown in Figure 8. Upon examination of the electroluminescent spectra of devices A, it was found that the emissions were mainly derived from Alq (λ_{max} = 530 nm). The emission of dyes appear as a minor component at a longer wavelength region (Figure 9). The CIE (Commission Internationale de l'Eclairage 1931) coordinates of these emissions therefore shifted substantially away from the region of normal red color.

The appearance of emission from Alq in device A can be ascribed to the migration of holes into the bulk of Alq layer, and annihilated with electrons there. The

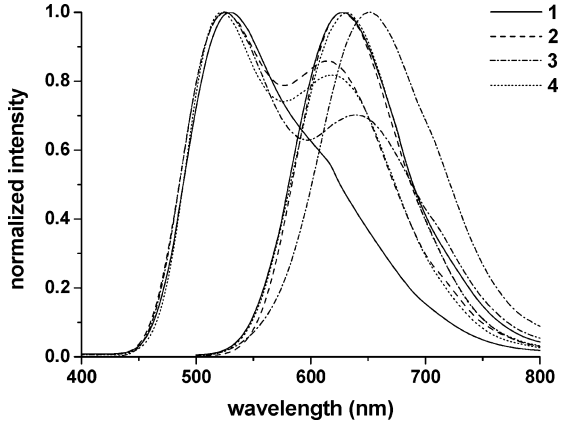

Figure 9. Electroluminescence spectra of **1**−**4**. The four spectra at left (λ_{max} = 530 nm) are emissions of device A, where the short wavelength components are derived from the emission of Alq. The four spectra at right are emissions of device B (λ_{em} = 627−650 nm), which are identical to the respective photoluminescence spectra.

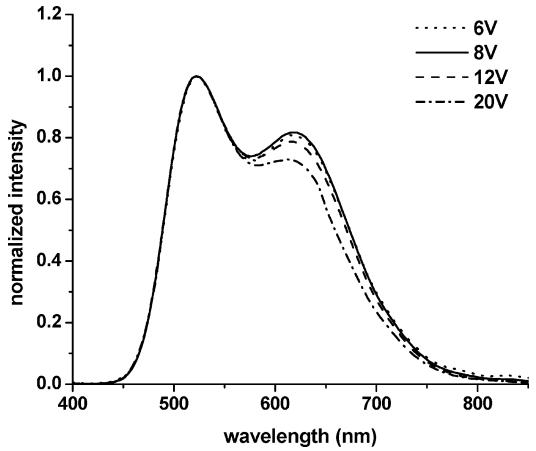

Figure 10. Electroluminescence spectra of compound **4** at different voltages of device A. At a higher voltage, e.g. 20 V, the relative intensity of the dye (at 620 nm) reduced slightly with respect to that of Alq (at 530 nm).

high efficiency of hole-transportation can be depicted by the voltage-dependent emission spectra of **4** (Figure 10). At higher bias the contribution of Alq to the emission spectrum was enriched because of an unbalanced rate of hole/electron migrations. The position of charge recombination can be tuned by replacing Alq with another electron-transporting material, i.e., TPBI. Because of the low HOMO level of TPBI, it is known to act as a hole-blocker in conjunction with NPB in a two-layer device configuration.[16] In device B the holes were successfully blocked at the interface between the dye and TPBI, so the charge recombination took place mostly within the boundary of the dye (Figure 11). The emission spectrum of device B (Figure 9) was found to be consistent with the photoluminescence of the corresponding dye (Figure 7).

The external quantum efficiency of **4** fabricated into both types of devices, A and B, reduced gradually along with increasing current density (Figure 12). However, the external quantum efficiencies of **1**−**3** were relatively

(16) (a) Koene, B. E.; Loy, D. E.; Thompson, M. E. *Chem. Mater.* **1998**, *10*, 2235. (b) Tao, Y.-T.; Balasubramaniam, E.; Danel, A.; Tomasik, P. *Appl. Phys. Lett.* **2000**, *77*, 933. (c) Balasubramaniam, E.; Tao, Y.-T.; Danel, A.; Tomasik, P. *Chem. Mater.* **2000**, *12*, 2788.

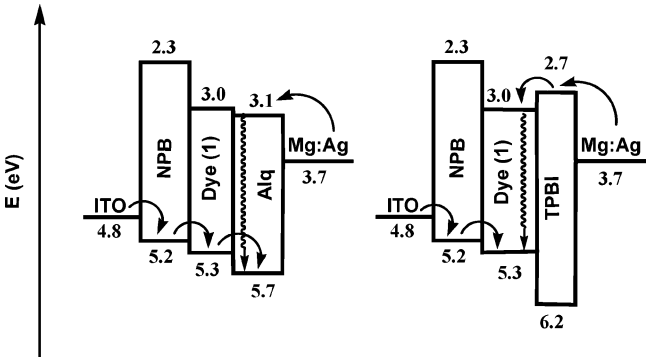

Figure 11. Relative energy levels in double heterojunction devices A (left) and B (right). In device A, holes were free to move into the bulk of Alq, and recombined with electrons there. In device B, TPBI acted as a hole blocker, so the charge recombination happened within the interface of TPBI and dye (e.g., **1**). The energy levels of NPB, Alq, and TPBI were quoted from ref 15c and d.

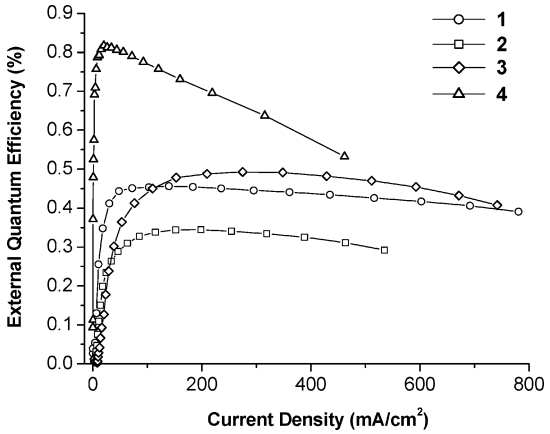

Figure 12. Plots of external quantum efficiency vs current density for devices B.

stable and did not show much reduction at higher current densities. It was commonly observed on red-color electrophosphorescent dyes that their efficiencies dropped rapidly at high current densities, due to either the effect of over saturation or triplet self-quenching.[8,17] The fluorescence decays of compounds **1**−**4** are quite fast, which renders the competitive quenching processes relatively insignificant. The performance of these devices has not yet been fully optimized.

The performance characteristics of devices A and B are summarized in Table 4. The performances of type A devices are slightly better than those of type B, however, the mixing of Alq emission in the former shifted the color from red to yellow-green. For devices of type B, red emissions with optimal brightness 1800−2400 cd/m^2 and external efficiencies 0.29−0.54% were achieved.

Table 4. Performance of Device A (ITO/NPB/1−4/Alq/Mg:Ag) and B (ITO/NPB/1−4/TPBI/Mg:Ag) Using Compounds 1−4 as Emitting Materials[a]

	turn-on (V)	luminance (Cd/m^2)	quantum efficiency	CIE coord.
		Device A		
1	3.0	9400 at 13 V	0.46% at 7 V	(0.38, 0.52)
2	5.2	3900 at 15 V	0.33% at 12 V	(0.41, 0.50)
3	4.4	7000 at 15 V	0.49% at 12 V	(0.39, 0.51)
4	2.0	5500 at 13 V	0.77% at 11 V	(0.42, 0.50)
		Device B		
1	3.0	2400 at 12 V	0.29% at 6 V	(0.61, 0.38)
2	3.9	1860 at 15 V	0.30% at 12 V	(0.62, 0.37)
3	3.6	1750 at 15 V	0.35% at 9 V	(0.63, 0.36)
4	2.0	1900 at 15 V	0.54% at 12 V	(0.61, 0.38)

[a] All four devices of type B exhibit red luminescence as indicated by their CIE coordinates, whereas those of type A exhibit yellow-green color.

Conclusions

It is demonstrated that bisindolylmaleimide derivatives **1**−**4** can be used as effective red electroluminescent materials. They were prepared readily by reactions of indolylmagnesium chloride with 2,3-dihalomaleimide. Their red color emission in solid state is ascribed to the formation of amorphous glasses which were evidenced by the observation of glass-transition temperatures on DSC. All compounds exhibit good thermal stability, and show reversible oxidation waves on CV. Typical devices configured as ITO/NPB/dye/TPBI/Mg:Ag showed turn-on voltages of 2−4 V, maximum luminance of 1800−2400 Cd/m^2 at about 13 V, and external quantum efficiency of 0.3−0.5%. On the CIE chromaticity scale all emissions are located within a range of (0.61−0.63, 0.36−0.38) which is very close to that of pure red.

Acknowledgment. Financial support from Academia Sinica and the National Science Council (NSC91-2113-M001-014) of the Republic of China are gratefully acknowledged. T.J.C. thanks the Institute for Fundamental Research of Organic Chemistry at Kyushu University for a visiting scholarship during the preparation of this manuscript.

Supporting Information Available: X-ray crystallographic files including atomic coordinates, bond lengths and angles, and anisotropic thermal parameters for **1** and **4** (PDF). This material is available free of charge via the Internet at http://pubs.acs.org.

CM0303890

(17) (a) O'Brien, D. F.; Baldo, M. A.; Thompson, M. E.; Forrest, S. R. *Appl. Phys. Lett.* **1999**, *74*, 442.